Spin and electronic excitations in 4f atomic chains on Au(111) substrates

David W. Facemyer,[1,*] Naveen K. Dandu,[2,3] Alex Taekyung Lee,[2,3] Vijay R. Singh,[2,3] Anh T. Ngo,[2,3] and Sergio E. Ulloa[1]

[1]*Department of Physics and Astronomy and Nanoscale and Quantum Phenomena Institute, Ohio University, Athens, Ohio 45701, USA*

[2]*Materials Science Division, Argonne National Laboratory, Lemont, Illinois 60439, USA*

[3]*Chemical Engineering Department, University of Illinois at Chicago, Chicago, Illinois 60608, USA*

(Received 14 December 2022; revised 8 June 2023; accepted 18 July 2023; published 4 August 2023)

High-spin systems, like those that incorporate rare-earth 4f elements, are increasingly relevant in many fields. Although research on such systems is sparse, the large Hilbert spaces they occupy are promising for many applications. In this work, we examine a one-dimensional linear array of europium atoms on a Au(111) surface and study their electronic and magnetic excitations. *Ab initio* calculations using VASP with the Perdew-Burke-Ernzerhof (PBE) functional + U are employed to study the structure. We find Eu atoms have a net charge when on gold, consistent with a net magnetic moment of $\simeq 3.5\mu_B$. Examining various spin-projection configurations, we can evaluate first- and second-neighbor exchange energies in an isotropic Heisenberg model between spin-$\frac{7}{2}$ moments to obtain $J_1 \approx -1.2$ K and $J_2 \approx 0.2$ K for a relaxed-chain atomic separation of $a \approx 5$ Å. These parameters are used to obtain the full spin excitation spectrum of a physically realizable four-atom chain. The large $|J_1|/J_2$ ratio results in a highly degenerate ferromagnetic ground state that is split by a significant easy plane single-ion anisotropy of 0.6 K. Spin-flip excitations are calculated to extract differential conductance profiles such as those obtained by scanning tunneling microscopy techniques. We uncover interesting behavior of local spin excitations, especially as we track their dispersion with applied magnetic fields.

DOI: 10.1103/PhysRevB.108.085407

I. INTRODUCTION

The study of low-dimensional arrays of localized magnetic moments, generally referred to as spin chains, is ubiquitous in physics. The simplicity of such systems resides only in their spatial dimension, however. The classical nature of spin chains is complex enough, but quantum mechanical effects enrich these systems even more. Many models and experiments have allowed us to gather information about the magnetic properties of spin chains, including their ground state and excitations, thermal magnetic properties, and possible phase transitions [1,2]. In the last decade research has also uncovered new exotic phenomena in atomic chains, such as building unique Kondo configurations [3] and creating Yu-Shiba [4] or Majorana edge states [5–7] whenever magnetic atoms are placed in proximity to superconducting substrates. In addition to the fundamental questions on the behavior of such interesting systems, a great deal of current research is rooted in technological advancement and possible applications, including quantum computing, the transmission of quantum information, and sensing [1,8].

Much of this work, however, has been focused on spin-$\frac{1}{2}$ systems, while larger-spin arrays have received much less attention. We consider here spin-$\frac{7}{2}$ magnetic moments such as those associated with some lanthanide (4f) atoms. The sorts of challenges and promises that come with these systems are easily recognized. Their Hilbert space grows rapidly with increasing site number (chain or cluster size), making these systems computationally expensive on classical computers. In contrast, these large Hilbert spaces may provide robust computational bases for quantum computation or information storage and a rich state manifold for complex dynamical behavior [9,10].

Scanning tunneling microscopy (STM) is a versatile and powerful tool for imaging atomic clusters or molecules on metallic surfaces. STM can further manipulate individual atoms or molecules on a substrate [11,12], allowing the design and construction of spin chains and clusters with precision, as well as the extraction of single-atom and collective electronic and magnetic properties [1,13]. The theoretical work we present here is motivated in part by these extraordinary capabilities, and it aims to provide insight into possible experiments on these deceptively simple structures.

Rare-earth elements are natural physical implementations of large-spin systems. For example, Gd^{+3} ions in $GdRh_2Si_2$ are well described experimentally as a pure spin-$\frac{7}{2}$ system [14]. The dynamic magnetic properties of core-shell nanowires of such a material were studied using an Ising model [15], while thermodynamic response functions were obtained using a three-state Blume-Capel model [16]. Similarly, the magnetic properties of La-substituted $Gd_{1-x}La_xRhIn_5$ were well characterized using a $\frac{7}{2}$ Heisenberg model for $x \leqslant 0.5$ [17]. Recent beautiful experiments exploring lanthanide atoms on thin insulating layers were able to modify [18] or measure [19] the magnetic moment of individual atoms, paving the way for many fundamental and practical questions using such systems. In addition, promising systems of rare-earth molecular complexes were studied recently [20].

*df008219@ohio.edu

A wide range of linear array candidates and the means for on-site manipulation also suggest deeper investigations into the realm of quantum information processing. A carefully tuned spin chain with strongly inhomogeneous couplings is predicted to exhibit perfect quantum information transfer [21]. Likewise, perfect state transmission over many chain sites was demonstrated in both XY and Heisenberg systems with local magnetic fields [22]. And quantum state transfer with high fidelity was predicted for large Heisenberg ferromagnetic chains [23]. To accurately substantiate such behavior in future experimental work, we must accurately obtain model parameters from a rather complex, but experimentally realizable, system, such as high-spin Eu ions on a Au(111) surface.

To explore such realistic systems, we utilize a combination of theoretical methods. Density functional theory (DFT), an indispensable tool to study the electronic structure of materials, provides us with the characteristic interactions between rare-earth atoms such as Eu deposited on a Au(111) surface. DFT finds a sizable charge and magnetic moment on each atom, compatible with spin-$\frac{7}{2}$, and allows us to extract nearest- and next-nearest-neighbor exchange energies in a Heisenberg model. Once these parameters are established, we explore a more experimentally realistic structure of an open-ended linear array of Eu atoms on the gold substrate. The low-energy magnetic excitation spectrum is obtained by exact diagonalization, which allows us to analyze the STM spectroscopy for site-specific spin excitations and their dependence on applied magnetic fields, as well as spatial correlations of the magnetic moments in the chain. The high symmetry of such a system results in low-energy manifolds with interesting magnetic field dependence. As strong fields cause increasing polarization of an otherwise singlet ferromagnetic ground state, the field-induced transitions are accompanied by characteristic changes in the differential conductance curves. Such behavior can be easily identified in experiments, providing a direct approach to the energetics of the system and benchmarking of system parameters. We also study the role of a possible noncolinear exchange interaction between magnetic moments and how it would affect the differential conductance curves. As the different interactions compete with one another in defining the excitation spectrum, they leave signatures that should assist in the full characterization of the overall low-energy dynamics of this rich spin system.

II. METHODS

A. First-principles calculations

Relaxation of a linear chain of Eu atoms on an Au(111) surface was carried out using the Vienna *Ab initio* Simulation Package (VASP) [24]. The valence electrons were described in terms of Kohn-Sham orbitals, expanded in a plane-wave basis with an energy cutoff of 500 eV. A Γ-centered k-point mesh of $8 \times 8 \times 1$ is used for all calculations. Atoms were allowed to relax until the net force per atom was less than 0.01 eV/Å. The supercell was 8×6, with three gold layers, with a vacuum layer thickness of 20 Å in the z direction. We have used the Perdew-Burke-Ernzerhof (PBE) functional + U with different values for U in Eu: 0, 3, and 7.2 eV. The electronic structure

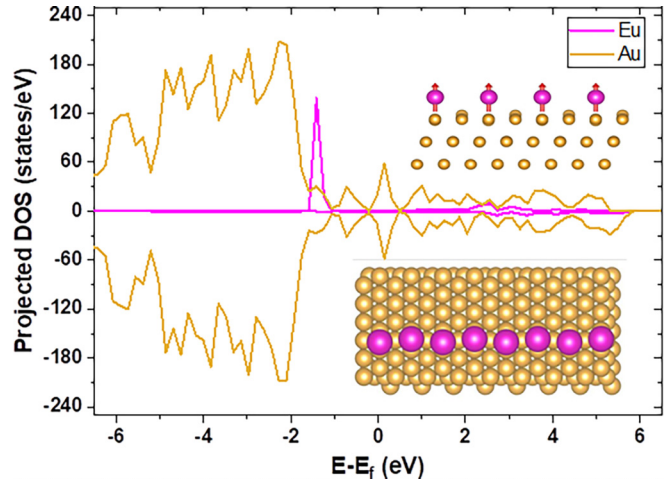

FIG. 1. Projected density of states near the Fermi level of model system for Eu and Au atoms using the PBE+U method with U = 3 eV (see [25] for other U values). Notice spin polarization of the Eu f orbital. The top inset shows the side view of a Eu atom linear chain on the Au(111) surface. The bottom inset shows the top view (two cells) of the system. The supercell has four Eu atoms and a gold slab with three layers. Eu-Eu average distance is 5.01 Å, and Eu-Au distance is 2.8 Å; interchain separation is 17.3 Å.

of Eu is qualitatively the same for different U values: Spin-up f bands are fully occupied, while spin-down bands are fully empty.

The simulated system supercell has four Eu atoms on the gold film with three atomic layers, with adatoms arranged in a way that makes the cell repeat periodically, as illustrated in the insets in Fig. 1. The bottom gold layer is kept fixed at the bulk lattice parameters, while the rest of the structure is allowed to relax. The electronic projected density of states (PDOS) near the Fermi level of the system indicates that all Eu ions have a well-defined magnetic moment (we find $\mu \simeq 3.5\mu_B$) as well as a Bader charge consistent with a 2+ ion (see Fig. 1). Figure S1 (see the Supplemental Material [25]) shows the PDOS of the same system using the different U values. As mentioned, increasing the value of U kept the magnetic moment on Eu unaltered; hereafter, we focus on the $U = 7.2$ eV case.

The formation energy of the system with $U = 7.2$ eV, calculated from the difference of separate subsystems, $\Delta\mathcal{E} = \mathcal{E}[4\,\text{Eu on Au(111)}] - \mathcal{E}[4\,\text{Eu}] - \mathcal{E}[\text{Au(111)}]$, is $\Delta\mathcal{E} = -12.6$ eV, suggesting the structure is stable. Comparing the energetics of various placements of a single Eu atom upon the substrate, we find that Eu adsorbed on the bridge of the Au atom gives the most favorable configuration. Table I compares different locations on gold for Eu atom placement. We should also note that the Eu atoms are not forced to stay in a linear chain. As the system relaxes, adatoms show no propensity to deform the chain. One notices a slight displacement from fully on-bridge locations in the final configuration, likely due to the presence of other Eu atoms.

Considering different magnetic configurations for the Eu ions along the chain, we find that the ferromagnetic configuration has the lowest energy, followed by the double-period

TABLE I. Energetics for different Eu atom adsorption sites on Au(111) using the PBE+U method with $U = 7.2$ eV.

Eu atom adsorption on different Au(111) sites	Relative energy (eV)
Bridge	0
Hollow hcp	0.2
On top	0.3
Hollow fcc	0.4

Néel arrangement, while the single-period Néel has the highest energy, as shown in Table II; U and D indicate maximal moment projections $\pm\frac{7}{2}$, respectively.

B. Heisenberg model

In order to extract effective exchange coupling constants, we consider an isotropic Heisenberg Hamiltonian and neglect local magnetic anisotropy [1,13]. The Hamiltonian is then

$$\hat{H} = \sum_{i<j} \hat{\vec{S}}_i \cdot \mathrm{J}_{ij} \cdot \hat{\vec{S}}_j, \tag{1}$$

where J_{ij} is the full magnetic exchange tensor that couples different pairs of effective moments. We consider first- and second-nearest-neighbor exchange coupling, so that the Hamiltonian takes the form

$$\begin{aligned}\hat{H}_{12} &= J_1 \sum_{\langle ij\rangle} \hat{\vec{S}}_i \cdot \hat{\vec{S}}_j + J_2 \sum_{\langle\langle ij\rangle\rangle} \hat{\vec{S}}_i \cdot \hat{\vec{S}}_j \\ &= J_1 \left(\sum_{\langle ij\rangle} \hat{\vec{S}}_i \cdot \hat{\vec{S}}_j + \alpha \sum_{\langle\langle ij\rangle\rangle} \hat{\vec{S}}_i \cdot \hat{\vec{S}}_j \right),\end{aligned} \tag{2}$$

where $\alpha = J_2/J_1$. Recall that $J_{ij} < 0$ corresponds to interacting moments favoring parallel alignment (i.e., ferromagnetic) and $J_{ij} > 0$ favors antiparallel (antiferromagnetic) alignment. One can estimate the coupling constants by evaluating the energy of corresponding configurations in Table II. Considering the energy for the four-atom supercell, one obtains

$$\begin{aligned} E_F &= \langle UUUU|\hat{H}_{12}|UUUU\rangle = 49J_1(\alpha+1), \\ E_N &= \langle UDUD|\hat{H}_{12}|UDUD\rangle = 49J_1(\alpha-1), \\ E_{dN} &= \langle UUDD|\hat{H}_{12}|UUDD\rangle = -49J_2. \end{aligned} \tag{3}$$

The energy differences between different configurations are then

$$\begin{aligned} \Delta E_1 &= E_N - E_F = -98J_1, \\ \Delta E_2 &= E_{dN} - E_F = -49J_1(1+2\alpha). \end{aligned} \tag{4}$$

TABLE II. Energy differences per unit cell with respect to the ferromagnetic ($UUUU$) ground state configuration for a Eu-ion linear chain on Au(111) using the PBE+U method with $U = 7.2$ eV.

Magnetic configuration	Total energy difference ΔE (meV)
$UDUD$	9.92
$UUDD$	2.89
$UUUU$	0

These equations, together with the corresponding energy differences from Table II, allow the determination of exchange energies, $J_1 \simeq -0.101$ meV ≈ -1.2 K and $J_2 \simeq +0.021$ meV ≈ 0.2 K. (The Supplemental Material shows exchange couplings as U values change [25].)

It is important to note that rare-earth ions have been shown to experience appreciable single-ion anisotropic (SIA) fields when adsorbed on coinage metal substrates [26]. We carried out Heyd-Scuseria-Ernzerhof functional with spin orbit coupling (HSE+SOC) calculations and found that a single Eu atom on Au(111) has magnetic easy plane anisotropy $A = 0.05$ meV $\approx$0.6 K, so that the low-energy Hamiltonian for the system is given by

$$\hat{H}_0 = J_1 \sum_{\langle ij\rangle} \hat{\vec{S}}_i \cdot \hat{\vec{S}}_j + J_2 \sum_{\langle\langle ij\rangle\rangle} \hat{\vec{S}}_i \cdot \hat{\vec{S}}_j + A \sum_i \left(\hat{S}_i^{(z)}\right)^2. \tag{5}$$

After extracting these parameters from the *ab initio* calculations, we employ full diagonalization of the Hamiltonian to explore the spin chain system characteristics, especially its response to external probes. We use QUSPIN [27] and focus here on an open chain with four Eu ions on the gold surface. Notice that the Hilbert space for N sites (magnetic moments) grows as 8^N due to the different spin projections, i.e., $m = \{\pm 7/2, \ldots, \pm 1/2\}$. The $N = 4$ chain with open boundary conditions allows us to capitalize on the inversion symmetry of the Hamiltonian and attain reasonable computational times. We can calculate the full magnetic excitation spectrum and corresponding eigenstates, as we discuss below.

III. MAGNETIC EXCITATIONS AND SPECTROSCOPY

A. Magnetic excitation spectrum

The large ratio $|J_1|/J_2 \simeq 5$ of this system suggests that the system should exhibit strongly ferromagnetic character throughout the low-lying excitation spectrum, with only a weak frustration induced by J_2. In the presence of only J_1 (taking $J_2 = A = 0$), the ground state has maximal spin $S = 14$ and corresponding high degeneracy (= 29). A weak J_2 does not change the ground state degeneracy but reduces the excitation gap to the $S = 13$ manifold from $\simeq 2|J_1|$ to $\simeq 0.8|J_1|$ [28] (see [25]).

The presence of SIA in Eq. (5) significantly affects the degeneracy of the $S = 14$ ground state, resulting in a nondegenerate "singlet" ($S_z = 0$) with ferromagnetic correlations and an interesting excitation pattern, as seen in Fig. 2. The first excited manifold is a degenerate doublet with $S_z = \pm 1$, followed by doublets with successively larger S_z components, $S_z = \pm 2, \pm 3, \pm 4$. The latter is closely spaced to another singlet ($S = 13$, $S_z = 0$) at $\simeq 2|J_1|$ above the ground state. The SIA interaction can be seen to produce shifts in the successive S_z doublets by an energy $\simeq \frac{1}{4}AS_z^2 \simeq \frac{1}{8}|J_1|S_z^2$ (Fig. 2).

B. STM spectroscopy

The rich structure of the magnetic excitation spectrum can be explored using different experimental probes. Ideally suited to carry this out is the differential spectroscopy technique using STM. By increasing bias voltage V while the STM tip is placed at different sites along the chain, one is able to excite different spin configurations that have a local overlap

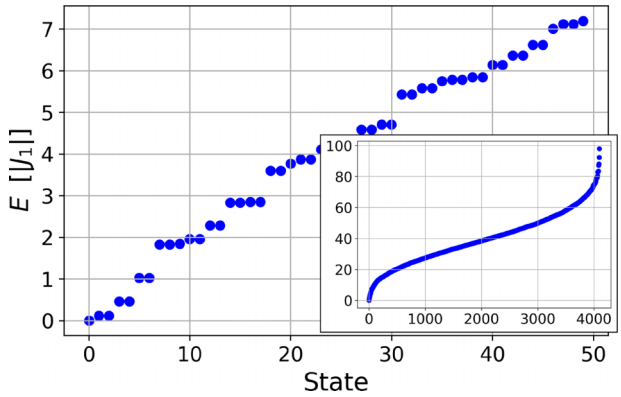

FIG. 2. Magnetic excitation spectrum for an open four-site spin chain of $S = 7/2$ magnetic moments with nearest- and next-nearest-neighbor exchanges, $J_1 = -0.101$ meV and $J_2 = 0.021$ meV, as well as an SIA contribution, $A = 0.05$ meV. The ground state is nondegenerate. The inset shows the full spectral range. Energies are in units of $|J_1|$.

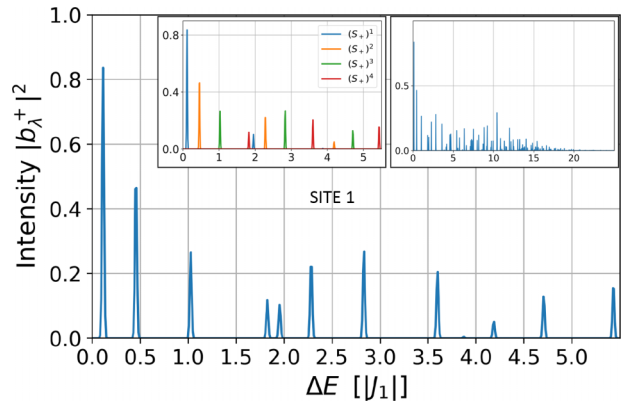

FIG. 3. Excitation profile for repeated spin raising on the first site of the Eu four-atom chain in its ferromagnetic singlet ground state. The left inset shows contributions to the main panel by successive spin "flips" on site 1—higher n appear at higher excitation energy. The right inset shows the higher-energy region. Weights are displayed using Gaussian broadening with FWHM $\simeq 0.02|J_1|$. All horizontal axes show excitation energy in units of $|J_1|$.

at that site which are reflected in differential conductance features as peaks in d^2I/dV^2 versus bias [1,13,29]. We can estimate theoretically what such an experiment will yield by considering the action of the tunneling electron producing spin-raising (or spin-lowering) events on the chain [29]. If the experiment is carried out at low temperatures, the system can be assumed to be in its ground state $|\Psi_{\text{grnd}}\rangle$. As the tunneling electrons go from the tip to the substrate (or vice versa), they can raise (S^+), lower (S^-), or leave unchanged (S^z) the magnetic moment of the structure they are tunneling through [29]. Notice that each tunneling electron can provide only angular momentum changes of $\pm\hbar$ (or zero) on the adsorbed species, so higher "spin flips" require repeated electron scatterings before relaxation and correspondingly higher tunneling currents.

Consider the action of the raising/lower spin operator on the ground state, $(S_i^{\pm})^n|\Psi_{\text{grnd}}\rangle = |\psi_i^{\pm(n)}\rangle$, which represents a local (on site i) magnetic excitation. This excitation can be seen as being composed of different excited eigenstates $|\lambda\rangle$, and one can write $|\psi_i^{\pm(n)}\rangle = \sum_\lambda b_\lambda^{\pm}|\lambda\rangle$. An example of the effect of successive spin-raising operator actions ($n = 1, \ldots, 4$) on the first atom of the chain is shown in Fig. 3, where the resulting weights $|b_\lambda^{\pm}|^2$ are plotted as a function of the excitation energy λ. The collection of weights provide an "excitation weight profile" for the system directly related to the differential conductance curves [30]. This profile provides an estimate of peak placement and relative intensities for the different transitions [31]. As the ground state of the chain is a nondegenerate $S_z = 0$ state, successive flips caused by the tunneling electrons can create excitations along the chain with an overall one quantum larger or smaller spin. Larger flips involve higher energy, reflecting the strong ferromagnetic correlations of the low-energy excitations. This provides distinct spectral signatures, as seen by the different colored curves in the top left inset in Fig. 3 for different n values in the case of the spin-raising operator $(S_i^+)^n$. The associated change in current versus bias voltage as different spin-flip channels open can easily be identified in experiments [31,32].

It is interesting to notice that tunneling onto different sites along the chain may change the differential conductance signatures. We find that the first and second sites of the chain have nearly identical spectral yield for low energy, likely again the result of the highly symmetric nondegenerate ground state. However, the amplitudes of various prominent high-energy peaks appear much higher when tunneling onto site 1 [25]. We emphasize that higher-energy excitations would be less likely at low tunneling current, resulting in an overall decaying probability envelope for higher energies [31]. Also note that the spatial inversion symmetry of the chain ensures the same results for tunneling onto the fourth and third sites. Similar behavior is seen for $(S^-)^n$ on different sites, as expected for an overall singlet ground state.

In what follows, we consider the effect of Zeeman fields on the spectrum of the system before discussing the weight profile as a function of field.

1. Zeeman field effects

Applying magnetic fields during STM spectroscopy experiments provides a powerful tool to obtain further information

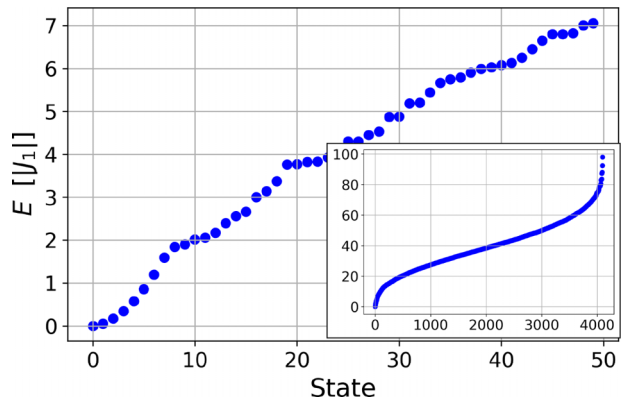

FIG. 4. Energy excitation spectrum for the four-site spin chain with Zeeman field $h_z = 0.1$ T. Notice the slight splitting of degenerate multiplets compared with those in Fig. 2.

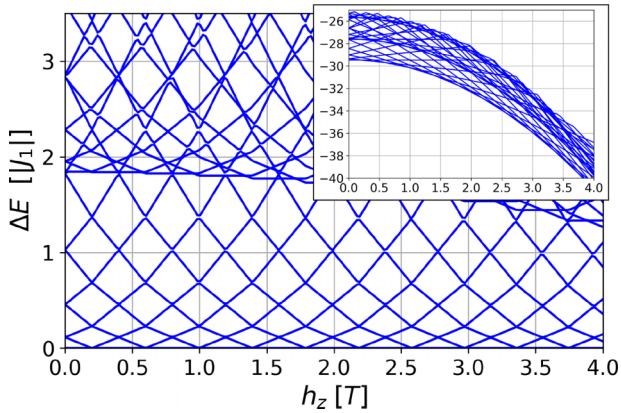

FIG. 5. Low-lying eigenstates for increasing applied Zeeman field. The ground state is polarized at increasing field from $S_z = 0$ to -1, -2, etc., at $h_z \simeq 0.2$, 0.6, etc. The main panel shows the lowest excitation energies. The inset shows linear splitting of different states, illustrating their S_z projection and tangent to a curved lower bound, i.e., the ground state.

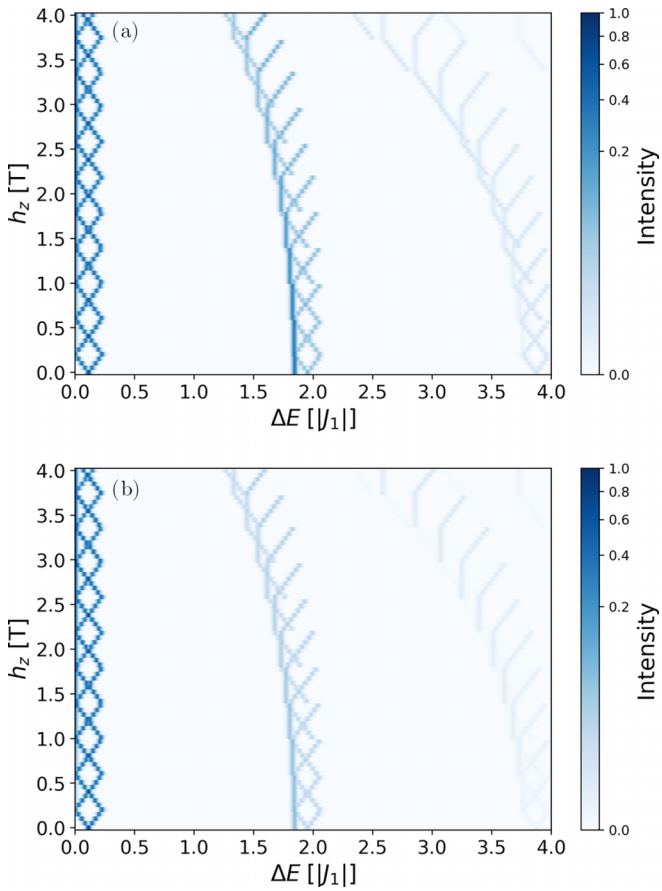

FIG. 6. Heat map of the excitation weight profile (approximately equal differential conductance signatures) for increasing Zeeman field strength and corresponding energy (bias). We show $I = 2|b^z|^2 + |b^+|^2 + |b^-|^2$ to account for all the different scattering processes for tunneling electrons as the energy/bias increases. Results for tunneling through the (a) first and (b) second sites. Tunneling through the second site produces weaker intensities, especially at higher-energy excitations and stronger fields, as seen in (b).

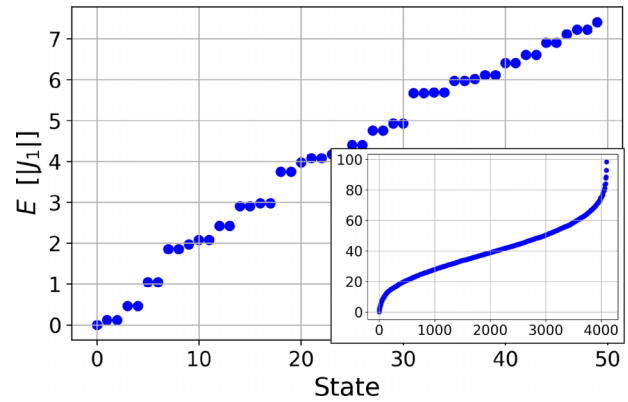

FIG. 7. Low-energy and full (inset) excitation spectrum for the four-site spin chain with $h_z = 0$ and $D_z = 0.1|J_1|$. Compare with Fig. 2.

on the system. A small field of $h_z = 0.1$ T splits degeneracies in the Eu chain for the low excitation energy manifolds, as shown in Fig. 4. The field splittings are linear, as the perturbing Hamiltonian is $\hat{H}_Z = h_z\hat{S}_z$, associated with the corresponding S_z total-spin projection of each state, so that the full Hamiltonian is

$$\hat{H} = \hat{H}_0 + h_z \sum_i \hat{S}_i^{(z)}, \tag{6}$$

with $\hat{H}_0$ from Eq. (5). The field dependence of the low-energy excitation spectrum is displayed in Fig. 5. The ground state of the chain is polarized from $S_z = 0$ to -1 at $h_z \gtrsim 0.2$ T, with decreasing S_z projection as h_z increases (to $S_z = -2$ at $\approx$0.6 T, etc.).

To explore the role of the Zeeman field in the differential conductance features, we calculate the excitation weight profile on the first and second sites of the chain as a function of field. As seen in the spectrum, the Zeeman coupling results in clear shifts with increasing field, as well as successive transitions to ever-increasing $|S_z|$ projection reflected well in the excitation weight profile. Figures 6(a) and 6(b) show profiles for single-scattering/tunneling events for sites 1 and 2, respectively. We see that the low-energy profiles for the different site excitations are rather similar, although much

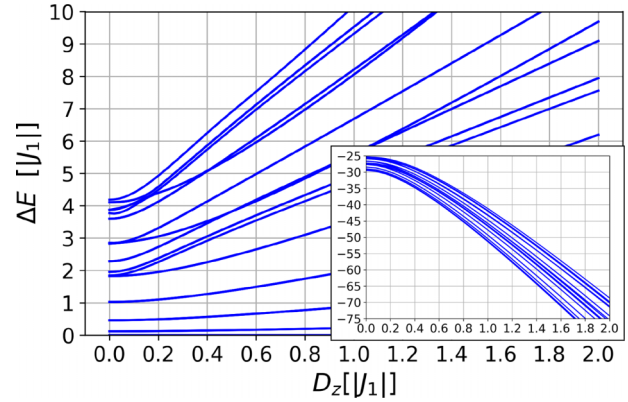

FIG. 8. Excitations for the Eu chain as D_z increases. The inset shows corresponding low-lying excitations, all for $h_z = 0$.

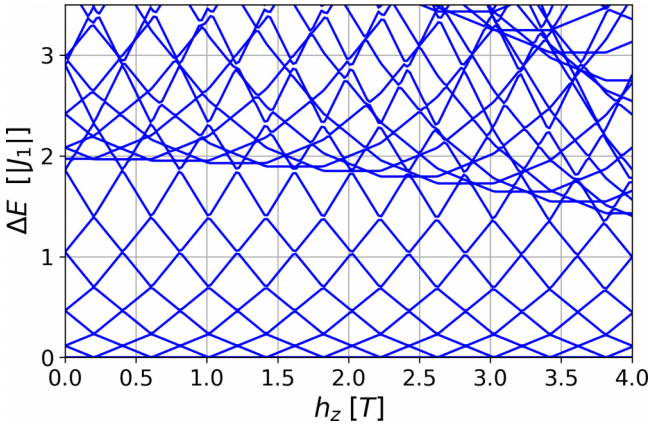

FIG. 9. Low-lying eigenstates for increasing applied Zeeman field and $D_z = 0.1|J_1|$ for the system in Fig. 2.

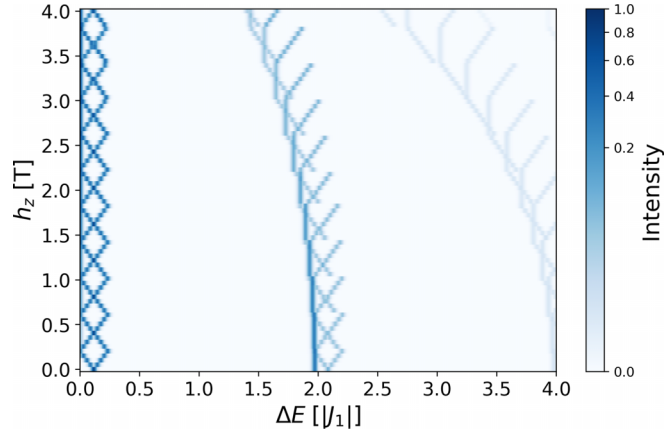

FIG. 10. Heat map of the excitation weight profile for increasing Zeeman field and the corresponding energy (bias) for the system with $D_z = 0.1|J_1|$ in Fig. 9. We plot $I = 2|b^z|^2 + |b^+|^2 + |b^-|^2$ to account for different scattering processes for tunneling electrons. Results are for tunneling through the first site.

weaker peaks at higher energy/bias are seen on site 2; this reflects the different environments of the two sites, which place site 2 more strongly in ferromagnetic order with the chain. For completeness, excitation weight profiles for higher-order scattering events are shown in [25,31].

2. Noncollinear exchange effects

It is reasonable to expect that a Dzyaloshinskii-Moriya interaction (DMI) may also appear in the spin system due to the strong Rashba spin-orbit effect measured on the gold surface [33]. This interaction results in the antisymmetric Hamiltonian $H_{\mathrm{DMI}} = \sum_{ij} \vec{D} \cdot \hat{\vec{S}}_i \times \hat{\vec{S}}_j$, which can qualitatively change the ground state configuration as well as the rest of the excitation spectrum [34–36]. To assess its effect on STM spectroscopy, we consider the likely dominant z component of the DMI vector $\vec{D}$. The full Hamiltonian then is

$$\hat{H} = \hat{H}_{\text{Eq. 6}} + \frac{iD_z}{2} \sum_{\langle ij \rangle} (\hat{S}_i^+ \hat{S}_j^- - \hat{S}_j^+ \hat{S}_i^-). \tag{7}$$

Figure 7 displays the resulting spectrum with $D_z = 0.1|J_1| = 0.01$ meV, showing that the ground state remains nondegenerate, while the excitation doublets are split more strongly the larger their $|S_z|$ values are; notice that the $\pm S_z$ degeneracies in the spectrum remain. Figure 8 shows how the excitation spectrum changes for larger D_z values, shifting all energies down as D_z increases, splitting degenerate manifolds, and producing some level crossings at high energy in the excitation spectrum with D_z (main panel).

We calculate the excitation weight profile as a function of Zeeman field for the system in Fig. 7, with field dependence shown in Fig. 9. Notice that the successively increasing polarization of the ground state appears here as well at lower Zeeman field strength. However, the $S_z = 0$ state in the second excitation manifold shifts from $\simeq 1.8|J_1|$ (Fig. 5) to about $2|J_1|$ for this D_z value. These shifts produce a general rightward bias (upward in energy) shift in the prominent peaks of the weight profiles in Fig. 10. Without DMI, these peaks begin at zero field near $\Delta E \simeq 1.8|J_1|$ and $\simeq 3.7|J_1|$; with DMI, they shift to start at $\Delta E \simeq 2$ and $\simeq 4|J_1|$, and the single-tunneling events at higher energy are somewhat stronger. In this case (not shown), tunneling through site 2 produces essentially the same differential conductance profile, indicating that the DMI has reduced the site asymmetry, as one would expect.

IV. CONCLUSIONS

The advent of atomic-site manipulation via STM has heralded a new era of materials science and engineering. One not only can design quantum systems but can also precisely assemble them and measure their electronic and magnetic characteristics at the level of a single atom or molecular entity. Spin chains, with a great history of deep insights into the physics of interacting systems, garner ever-increasing interest as they naturally interface with the growing fields of quantum information transmission, computing, and sensing. Our proposal to assemble large-spin systems to highlight their rich behavior focused on a four-atom chain of effective Eu^{2+} ions on a Au(111) surface. First-principles calculations of realistic systems allowed us to extract magnetic excitation spectra and the resulting differential conductance profiles with site-specific excitations. Experimental realization of this system not only would provide us with the interesting opportunity of benchmarking our model and specific exchange parameters but would also be the next step in exploring quantum information transfer down long chains.

ACKNOWLEDGMENTS

We thank S.-W. Hla and E. Masson for helpful discussions and acknowledge financial support from the U.S. Department of Energy, Office of Science, Office of Basic Energy Sciences, Materials Science and Engineering Division.

[1] D.-J. Choi, N. Lorente, J. Wiebe, K. von Bergmann, A. F. Otte, and A. J. Heinrich, Colloquium: Atomic spin chains on surfaces, Rev. Mod. Phys. **91**, 041001 (2019).

[2] H.-J. Mikeska and A. K. Kolezhuk, One-dimensional magnetism, in *Quantum Magnetism*, edited by U. Schollwöck, J. Richter, D. J. J. Farnell, and R. F. Bishop (Springer, Berlin, 2004), pp. 1–83.

[3] D.-J. Choi, R. Robles, S. Yan, J. A. J. Burgess, S. Rolf-Pissarczyk, J.-P. Gauyacq, N. Lorente, M. Ternes, and S. Loth, Building complex Kondo impurities by manipulating entangled spin chains, Nano Lett. **17**, 6203 (2017).

[4] M. Ruby, B. W. Heinrich, Y. Peng, F. von Oppen, and K. J. Franke, Wave-Function Hybridization in Yu-Shiba-Rusinov Dimers, Phys. Rev. Lett. **120**, 156803 (2018).

[5] S. Nadj-Perge, I. K. Drozdov, J. Li, H. Chen, S. Jeon, J. Seo, A. H. MacDonald, B. A. Bernevig, and A. Yazdani, Observation of Majorana fermions in ferromagnetic atomic chains on a superconductor, Science **346**, 602 (2014).

[6] M. Ruby, B. W. Heinrich, Y. Peng, F. von Oppen, and K. J. Franke, Exploring a proximity-coupled Co chain on Pb(110) as a possible Majorana platform, Nano Lett. **17**, 4473 (2017).

[7] H. Kim, A. Palacio-Morales, T. Posske, L. Rózsa, K. Palotás, L. Szunyogh, M. Thorwart, and R. Wiesendanger, Toward tailoring Majorana bound states in artificially constructed magnetic atom chains on elemental superconductors, Sci. Adv. **4**, eaar5251 (2018).

[8] C. D. Bruzewicz, J. Chiaverini, R. McConnell, and J. M. Sage, Trapped-ion quantum computing: Progress and challenges, Appl. Phys. Rev. **6**, 021314 (2019).

[9] S. Brinker, F. Küster, S. S. P. Parkin, P. Sessi, and S. Lounis, Anomalous excitations of atomically crafted quantum magnets, Sci. Adv. **8**, eabi7291 (2022).

[10] A. Scheie, P. Laurell, B. Lake, S. E. Nagler, M. B. Stone, J.-S. Caux, and D. A. Tennant, Quantum wake dynamics in Heisenberg antiferromagnetic chains, Nat. Commun. **13**, 5796 (2022).

[11] S.-W. Hla, Scanning tunneling microscopy single atom/molecule manipulation and its application to nanoscience and technology, J. Vac. Sci. Technol., B **23**, 1351 (2005).

[12] Z. Majzik, N. Pavliček, M. Vilas-Varela, D. Pérez, N. Moll, E. Guitián, G. Meyer, D. Peña, and L. Gross, Studying an antiaromatic polycyclic hydrocarbon adsorbed on different surfaces, Nat. Commun. **9**, 1198 (2018).

[13] M. Ternes, Spin excitations and correlations in scanning tunneling spectroscopy, New J. Phys. **17**, 063016 (2015).

[14] K. Kliemt, M. Hofmann-Kliemt, K. Kummer, F. Yakhou-Harris, C. Krellner, and C. Geibel, $GdRh_2Si_2$: An exemplary tetragonal system for antiferromagnetic order with weak in-plane anisotropy, Phys. Rev. B **95**, 134403 (2017).

[15] M. Ertaş, Dynamic magnetic properties of the spin-7/2 Ising nanowire systems with core–shell structure, Eur. Phys. J. Plus **137**, 178 (2022).

[16] M. Karimou and M. Bati, Magnetic properties of spin-7/2 Blume-Capel chain under a magnetic field, Solid State Commun. **324**, 114137 (2021).

[17] R. Lora-Serrano, D. J. Garcia, D. Betancourth, R. P. Amaral, N. S. Camilo, E. Estévez-Rams, L. A. Ortellado G. Z., and P. G. Pagliuso, Dilution effects in spin 7/2 systems. the case of the antiferromagnetic $GdRhIn_5$, J. Magn. Magn. Mater. **405**, 304 (2016).

[18] F. D. Natterer, K. Yang, W. Paul, P. Willke, T. Choi, T. Greber, A. J. Heinrich, and C. P. Lutz, Reading and writing single-atom magnets, Nature (London) **543**, 226 (2017).

[19] M. Ternes, C. P. Lutz, A. J. Heinrich, and W.-D. Schneider, Sensing the Spin of an Individual Ce Adatom, Phys. Rev. Lett. **124**, 167202 (2020).

[20] T. M. Ajayi, V. Singh, K. Z. Latt, S. Sarkar, X. Cheng, S. Premarathna, N. K. Dandu, S. Wang, F. Movahedifar, S. Wieghold, N. Shirato, V. Rose, L. A. Curtiss, A. T. Ngo, E. Masson, and S. W. Hla, Atomically precise control of rotational dynamics in charged rare-earth complexes on a metal surface, Nat. Commun. **13**, 6305 (2022).

[21] P. Karbach and J. Stolze, Spin chains as perfect quantum state mirrors, Phys. Rev. A **72**, 030301(R) (2005).

[22] M. Christandl, N. Datta, A. Ekert, and A. J. Landahl, Perfect State Transfer in Quantum Spin Networks, Phys. Rev. Lett. **92**, 187902 (2004).

[23] S. Bose, Quantum Communication through an Unmodulated Spin Chain, Phys. Rev. Lett. **91**, 207901 (2003).

[24] G. Kresse and J. Furthmüller, Efficiency of *ab-initio* total energy calculations for metals and semiconductors using a plane-wave basis set, Comput. Mater. Sci. **6**, 15 (1996).

[25] See Supplemental Material at http://link.aps.org/supplemental/10.1103/PhysRevB.108.085407 for additional results for other U values, spectra and spin correlations, as well as full tunneling map.

[26] T. Schuh, T. Miyamachi, S. Gerstl, M. Geilhufe, M. Hoffmann, S. Ostanin, W. Hergert, A. Ernst, and W. Wulfhekel, Magnetic excitations of rare earth atoms and clusters on metallic surfaces, Nano Lett. **12**, 4805 (2012).

[27] P. Weinberg and M. Bukov, QuSpin: A Python package for dynamics and exact diagonalisation of quantum many body systems part I: Spin chains, SciPost Phys. **2**, 003 (2017).

[28] It is suggestive to note that the competition between neighbor exchange energies may be related to the indirect exchange mediated by the Au(111) electrons. The Fermi wavelength for the surface state in Au(111), $\lambda_F \simeq 36$ Å [37], agrees well with the intrachain atomic spacing ($\simeq$5 Å) and may be partially responsible for producing the exchange couplings with alternating signs.

[29] F. Delgado, J. J. Palacios, and J. Fernández-Rossier, Spin-Transfer Torque on a Single Magnetic Adatom, Phys. Rev. Lett. **104**, 026601 (2010).

[30] R. Toskovic, R. van den Berg, A. Spinelli, I. S. Eliens, B. van den Toorn, B. Bryant, J. S. Caux, and A. F. Otte, Atomic spin-chain realization of a model for quantum criticality, Nat. Phys. **12**, 656 (2016).

[31] The visibility of spin excitations will depend on the tunneling current intensity as $\simeq I^n$, so that higher spin flips will require higher currents to occur with sufficient amplitude. Variation of STM set points can provide information on these features.

[32] A. J. Heinrich, J. A. Gupta, C. P. Lutz, and D. M. Eigler, Single-atom spin-flip spectroscopy, Science **306**, 466 (2004).

[33] M. Hoesch, M. Muntwiler, V. N. Petrov, M. Hengsberger, L. Patthey, M. Shi, M. Falub, T. Greber, and J. Osterwalder, Spin

structure of the Shockley surface state on Au(111), Phys. Rev. B **69**, 241401(R) (2004).

[34] I. Dzyaloshinsky, A thermodynamic theory of "weak" ferromagnetism of antiferromagnetics, J. Phys. Chem. Solids **4**, 241 (1958).

[35] T. Moriya, Anisotropic superexchange interaction and weak ferromagnetism, Phys. Rev. **120**, 91 (1960).

[36] E. Vernek, O. Ávalos-Ovando, and S. E. Ulloa, Competing interactions and spin-vector chirality in spin chains, Phys. Rev. B **102**, 174427 (2020).

[37] K. Sotthewes, M. Nijmeijer, and H. J. W. Zandvliet, Confined Friedel oscillations on Au(111) terraces probed by thermovoltage scanning tunneling microscopy, Phys. Rev. B **103**, 245311 (2021).